



**Anomalous thermoelectricity at the two-dimensional structural transition of SnSe monolayers**John W. Villanova <sup>\*</sup> and Salvador Barraza-Lopez <sup>†</sup>*Department of Physics, University of Arkansas, Fayetteville, Arkansas 72701, USA*

(Received 22 October 2020; accepted 4 January 2021; published 21 January 2021)

The thermoelectric figure of merit  $ZT$  comprises *electronic* and *vibrational* contributions that drastically change across phase transitions, and the most common theoretical *ab initio* approach to thermoelectricity fails to describe the evolution of  $ZT$  across finite-temperature structural transitions in its entirety. Furthermore, while the thermoelectric behavior of *bulk* SnSe has been extensively studied, SnSe *monolayers* have been experimentally realized only recently, and the existent prediction of thermoelectricity on this two-dimensional material is unreliable because it misses its structural transition altogether. SnSe monolayers (and similar GeS, GeSe, GeTe, SnS, and SnTe monolayers) experience a temperature-induced two-dimensional  $Pnm2_1 \rightarrow P4/nmm$  structural transition precipitated by the softening of vibrational modes, and we describe their thermoelectric properties across the phase transition, using molecular dynamics data to inform both electronic and vibrational coefficients directly and within the same footing. Similar to recent experimental observations pointing to an overestimated  $ZT$  past the transition temperature in bulk SnSe, we find a smaller  $ZT$  on SnSe monolayers when compared to its value predicted by the standard paradigm, due to the dramatic changes in the electrical conductivity and lattice thermal conductivity as the structural transition ensues. The process described here lends a strong focus to both the vibrational and electronic evolutions throughout the structural transition, and it applies to thermoelectric materials undergoing thermally driven solid-to-solid structural phase transitions in one, two, and three dimensions.

DOI: [10.1103/PhysRevB.103.035421](https://doi.org/10.1103/PhysRevB.103.035421)**I. INTRODUCTION**

The theory of thermoelectricity has clear mandates for improvement when the community observes that “finding ways to move beyond our current reliance on the *ground state electronic and phonon band structures* will be key to future progress in this area” [1]. Bulk SnSe has been argued to display an extremely large thermoelectric figure of merit  $ZT$  at its thermally driven  $Pnma \rightarrow Cmcm$  structural transition [2–7]. Nevertheless, the existence of such a high  $ZT$  has been put in doubt recently [8–10]: The lattice thermal conductivity  $\kappa_l$  appears to be seriously underestimated throughout the structural transition.

SnSe monolayers are structurally stable binary semiconductors with an intrinsic in-plane electric dipole moment in their ground-state  $Pnm2_1$  structural configuration [11,12]. While bulk SnSe undergoes a phase transition at temperatures as high as 900 K [13], SnSe monolayers on graphite display a critical temperature closer to 400 K [11]. A previous study of the thermoelectric properties of freestanding SnSe monolayers did not address the effect of the structural transition on thermoelectric properties [14]. Here, we discuss a process to capture the effects of phase transitions on thermoelectric properties, and exemplify it on this two-dimensional material.

The thermoelectric figure of merit is given by [1,15]

$$ZT = \frac{\sigma S^2 T}{\kappa_e + \kappa_l}, \quad (1)$$

where  $\sigma$  is the electrical conductivity,  $S$  is the Seebeck coefficient,  $T$  is the temperature, and  $\kappa_e$  is the electronic contribution to the thermal conductivity. Here, we determine the thermoelectric figure of merit  $ZT$  across a thermally driven structural phase transition relying directly on structural data obtained at finite  $T$ . As a result, we predict a sudden increase in  $\sigma$ ,  $\kappa_e$ , and  $\kappa_l$  across the structural transition [16,17], and  $ZT$  decreases substantially near the onset of the structural transition. In line with recent experimental results obtained for bulk (3D) thermoelectric materials [9,10], our findings put to question record high values of  $ZT$  (in excess of 3 [14]) on materials undergoing structural phase transitions. Though exemplified in a two-dimensional (2D) ferroelectric, the process applies to any material undergoing solid-to-solid structural transitions.

The manuscript is structured as follows: The computational methods are introduced in Sec. II. Numerical results, and a discussion of the process to obtain the lattice thermal conductivity from molecular dynamics data are contained in Sec. III. Conclusions are offered in Sec. IV.

**II. METHODS**

*Ab initio* molecular dynamics (MD) calculations on (2D) SnSe monolayers employing the SIESTA code [18] were carried out on a  $16 \times 16 \times 1$  supercell containing 1024 atoms within the isothermal-isobaric ( $NPT$ ) ensemble. We captured dynamics over 28 000 fs for more than 10 temperatures between 0 and 400 K with a 1.5-fs time resolution. The out-of-plane lattice vector had a length of 22 Å to ensure no interaction between periodic copies (see Refs. [12,16,17,19–21] for additional details). We took the average structure from

<sup>\*</sup>jvillano@uark.edu<sup>†</sup>sbarraza@uark.edu

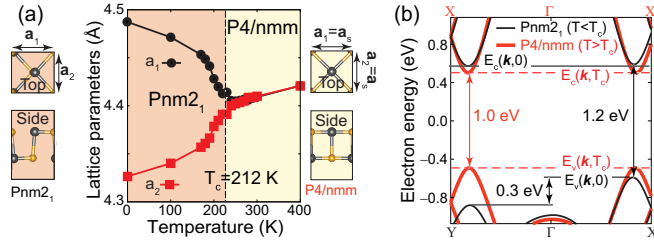


FIG. 1. (a) Thermal evolution of in-plane lattice parameters  $a_1$  and  $a_2$  for a freestanding SnSe monolayer, demonstrating a structural transition from an orthorhombic ( $Pnm2_1$ ) unit cell onto a unit cell with tetragonal ( $P4/nmm$ ) symmetry at  $T_c = 212$  K [16,17]. Top and side views of the atomistic arrangements are shown, too. (b) Evolution of the valence ( $v$ ) and conduction ( $c$ ) bands of the SnSe monolayer as a result of the transition.

each temperature in the MD calculation and used SIESTA to calculate Hamiltonian and overlap matrices. The electronic transport coefficients were obtained using Boltzmann transport theory on average unit cells at finite temperature [15,22].

The lattice thermal conductivity  $\kappa_l$  was also obtained from the finite-temperature MD evolution using a process delineated in Sec. III. For comparison purposes, the SHENGBTE code [22] was used to calculate  $\kappa_l$ ; the interatomic forces were calculated using the same settings employed in SIESTA on a  $5 \times 5 \times 1$  supercell with up to third nearest neighbors for the third-order force constants. We used a  $36 \times 36 \times 1$   $k$ -point mesh and a SCALEBROAD parameter of 1.0.

### III. RESULTS AND DISCUSSION

Figure 1(a) displays the average lattice parameters  $a_1$  and  $a_2$  of a freestanding SnSe monolayer as a function of  $T$ . A fit of critical exponents yields  $T_c = 212$  K [16] (the larger experimental value of 400 K [11] is attributed to the interaction of the SnSe monolayer with its supporting substrate). The SnSe monolayer turns paraelectric at  $T \geq T_c$ , as the unit cell develops a fourfold symmetry consistent with the  $P4/nmm$  space group. Figure 1(a), experiment [11], and the fact that the standard thermoelectric theory relies on zero-temperature structural data all demonstrate that an incorrect atomistic symmetry ( $Pnm2_1$ ) was previously employed to determine the thermoelectric properties of a SnSe monolayer within the reported 300–700 K temperature range [14,23,24].

Setting the focus on dimensionality aside for a moment and giving context for our approach, two articles resemble the methodology proposed here. In Ref. [6] the authors use a supercell with 256 atoms and the  $NVT$  ensemble. Their electronic contributions to  $ZT$  show a sharp discontinuity at 750 K (when pressure is 0 GPa) or at 500 K (when pressure is 4 GPa); this ensues because of the use of two atomistic structures (with either  $Pnma$  or  $Cmcm$  symmetry) to compute these quantities. While the electronic contributions to  $ZT$  are computed for temperatures up to 1000 K, the lattice thermal conductivity is computed within a smaller (200 to 500 K) temperature range, and  $ZT$  was not estimated. The second work is Ref. [7]. There, three structures are used to inform the Seebeck coefficient over a 900 K temperature range and read directly from experimental data [13] at 298, 790, and 825 K.

The fact that only two references (out of so many devoted to bulk SnSe) discuss the effect of a changing atomistic structure on thermoelectric properties reinforces the observation that common paradigms are failing to describe the evolution of thermoelectric properties across phase transitions, and the use of finite- $T$  information straight from *ab initio* molecular dynamics to determine all thermoelectric properties is delineated next.

Structural changes modify the electronic bands: The electronic structure shown in black in Fig. 1(b) corresponds to the  $Pnm2_1$  atomistic structure at  $T = 0$ ; that is, to the electronic structure employed at all temperatures (300 to 700 K) in works that rely on the standard *ab initio* formalism for thermoelectricity (e.g., Refs. [14,23,24] for the SnSe monolayer at hand). The electronic bands shown in red in Fig. 1(b) correspond to the average atomistic structure of the freestanding SnSe monolayer above 212 K. The two hole valleys turn degenerate due to the enhanced tetragonal symmetry of the  $P4/nmm$  space symmetry group. In what follows, the electronic band structure is labeled  $E_\alpha(\mathbf{k}, T)$ , where  $\alpha$  is the band index, to emphasize its dependence on the average unit cell at finite  $T$ .

The temperature dependence of  $\sigma$  in the standard *ab initio* approach to thermoelectricity [15,22] enters only through a scattering time  $\tau$  and through the Fermi-Dirac distribution  $f(E - \mu, T)$ . Here, however,  $\sigma_{ij}$  incorporates the finite- $T$  dependence of the electron group velocities  $\mathbf{v}_\alpha$  for band  $\alpha$ , and of the unit cell area as well through the use of the average unit cell as obtained from the molecular dynamics data at finite  $T$ :

$$\sigma_{ij}(T) = \frac{e^2}{\Omega(T)} \sum_{\mathbf{k}, \alpha} v_{\alpha,i}(\mathbf{k}, T) v_{\alpha,j}(\mathbf{k}, T) \tau_e(T) g(E, \mu, T), \quad (2)$$

where  $g(E, \mu, T) = -\frac{\partial f(E - \mu, T)}{\partial E}$ ,  $i = x, y$  and  $j = x, y$  represent Cartesian directions,  $e$  is the electron charge, and  $\hbar$  is the reduced Planck constant.  $\Omega(T) = a_1(T)a_2(T)L(T)$  (with  $L(T)$  the material thickness) is the  $T$ -dependent volume of the unit cell,  $\tau_e$  is the electron relaxation time, and  $v_{\alpha,i}(\mathbf{k}, T) = \frac{1}{\hbar} \frac{\partial E_\alpha(\mathbf{k}, T)}{\partial k_i}$  is the band group velocity. ( $\alpha$  is a band index, and  $i, j$  label cartesian ( $x, y$ ) components.) Although the electron relaxation time  $\tau_e$  may also be  $T$  dependent, a  $T$ -independent magnitude of  $10^{-14}$  s is assigned in accordance with previous estimates [4,14,24–26]. It may be appropriate to indicate that, for consistency, we did not pursue an atomistic optimization of the atoms on the average unit cell we obtained at finite temperature.

Figure 2(a) showcases, with dashed (dash-dotted) lines, the electron (hole) conductivity with  $\mu$  at the conduction (valence) band edge using a zero- $T$  relaxed volume and zero- $T$  electronic structure (standard paradigm [15,22]) to compare against the predictions from this method. The  $T$ -dependent method deployed here, shown by solid lines and red squares (black circles) for the valence (conduction) band edge, tracks closely with the dashed-dot curves for  $T < T_c$ , but it is smaller than the electronic contribution as determined from the standard paradigm (dashed curves). There is a marked increase in  $\sigma$  at  $T_c$  in our calculations as the electron (hole) pockets of the conduction (valence) band align due to an increased symmetry above  $T_c$  (Fig. 1(b)). For  $T > T_c$ , the standard paradigm predicts greater electron conductivity compared to hole

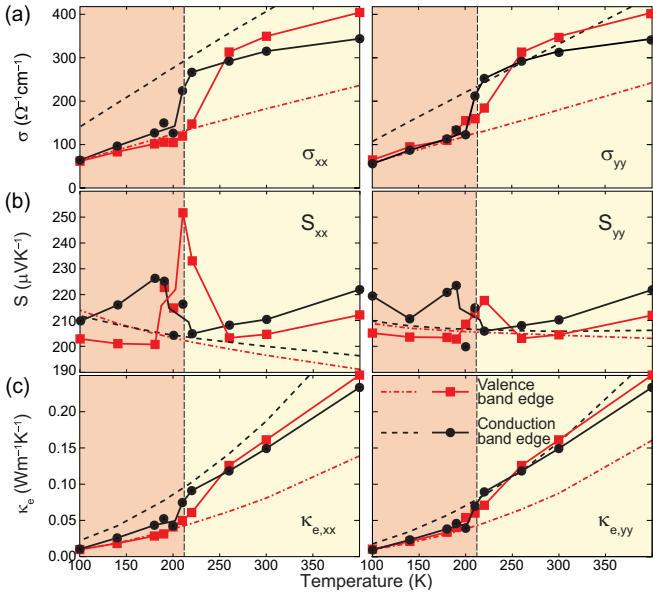


FIG. 2. (a) Electrical conductivity  $\sigma$ , (b)  $S$ , and (c)  $\kappa_e$  along the  $\mathbf{a}_1$  ( $x$ ) and  $\mathbf{a}_2$  ( $y$ ) directions versus  $T$  for  $\mu$  set at the conduction and valence band edges. Note the upticks at  $T_c$  due to a temperature-induced band alignment and the enhanced symmetry past  $T_c$ , both absent features in the standard approach [15,22] that takes electronic band structures on the ground state ( $T=0$  K) atomistic structures for temperatures below and above the transition (dashed and dash-dotted curves).

conductivity, but our  $T$ -dependent formalism indicates the opposite trend for  $T \geq 250$  K. (Work on bulk SnSe displays a similar increase in carrier concentration (electrical conductivity) induced by the transition [2,7], but the observed behavior of  $\sigma$  was assigned to the creation of Sn vacancies [7]).

We next account for the Seebeck coefficient  $S$ , obtained by dividing the expression

$$[\sigma S(T, \mu)]_{ij} = \frac{-e}{T\Omega(T)} \sum_{\mathbf{k}, \alpha} v_{\alpha,i}(\mathbf{k}, T) v_{\alpha,j}(\mathbf{k}, T) \times \tau_{e,g}(E, \mu, T) [E_{\alpha}(\mathbf{k}, T) - \mu] \quad (3)$$

by Eq. (2).  $S$ , as depicted in Fig. 2(b), was computed with  $\mu$  set at either the valence or conduction band edges. As was the case for  $\sigma$ ,  $S$  is asymmetric in the usual formalism. It exhibits a peak at  $T_c$  for  $S_{xx}$  and a subdued peak for  $S_{yy}$ . When contrasted with the temperature evolution of  $\sigma$ ,  $S$  is otherwise roughly constant over the temperature range investigated, showing an increase and a subsequent decrease as in bulk samples [7,13].

The denominator in Eq. (1) contains the electronic ( $\kappa_e$ ) and lattice ( $\kappa_l$ ) contributions to the thermal conductivity. The  $\kappa_{e,ij}$  tensor has two terms,

$$\kappa_{e,ij}(T, \mu) = \mathcal{K}_{ij}(T, \mu) - T[\sigma S(T, \mu)]_{ij}^2 \sigma(T, \mu)_{ij}^{-1}, \quad (4)$$

with the first contribution being

$$\mathcal{K}_{ij}(T, \mu) = \frac{1}{T\Omega(T)} \sum_{\mathbf{k}, \alpha} v_{\alpha,i}(\mathbf{k}, T) v_{\alpha,j}(\mathbf{k}, T) \times \tau_{e,g}(E, \mu, T) [E_{\alpha}(\mathbf{k}, T) - \mu]^2 \quad (5)$$

and the second term expressible from Eqs. (2) and (3).  $\kappa_e$  [Fig. 2(c)] displays a trend similar to the one observed for  $\sigma$  in Fig. 2(a). Transport coefficients turn symmetric past  $T_c$ , which could serve as an experimental signature to verify whether this finite- $T$  approach to thermoelectricity surpasses the state of the art. Calculating  $\kappa_l$  requires additional methods to collect phonon frequencies and lifetimes from the MD data, which we present next.

In materials at the onset of structural transitions [27–29], “anharmonicity drives the crystal past the zero-temperature structure onto a new crystalline phase for which the zero-temperature electronic and zero-temperature phonon dispersions may no longer carry meaning” [30]. There have been vigorous efforts to account for temperature-dependent effects on  $ZT$  [6,7,31–34], yet most *ab initio* thermoelectricity works ignore structural transitions altogether (see, e.g., Refs. [14,15,22–24,35]); these modifications have certainly not been employed to discuss 2D thermoelectrics yet. Here, the challenge is met by using the power spectrum of the vibrational modes derived from molecular dynamics by way of the velocity autocorrelation function; the approach applies to thermoelectric materials in 1, 2 and 3 spatial dimensions.

Figure 3(a) displays the  $16 \times 16$  first Brillouin zone and the  $k$ -point sampling achieved without interpolation on the 1024-atom  $16 \times 16$  supercell employed in our molecular dynamics calculations [36]. The high- $T$  ( $P4/nmm$ ) phase is fourfold symmetric [17], making the  $X$  and  $Y$  points equivalent. A power spectrum at each  $k$ -point is obtained by Fourier transforming the velocities of the atoms into reciprocal space, performing the time autocorrelation, and then Fourier transforming into frequency space [37]. This process yields the finite temperature resonant natural frequencies  $\nu_{\alpha}(\mathbf{k}, T)$ , as demonstrated by the black curves for two nearby  $k$ -points  $\mathbf{k}$  at  $T = 100$  K ( $< T_c$ ) and 230 K ( $> T_c$ ) in Fig. 3(b). The finite- $T$  phonon dispersions of the freestanding SnSe monolayer along the red path in Fig. 3(a) are shown in Fig. 3(c). We observe a softening of vibrational modes along the Brillouin zone boundary at frequencies between 2 and 4 THz for  $T > T_c$  [17] in Figs. 3(b) and 3(c): these softened vibrational modes will effect an increase on  $\kappa_l$ , and a subsequent decrease on  $ZT$ .

The central frequencies  $\nu_{\alpha}(\mathbf{k}, T)$  and the full width at half maximum  $\Delta\nu_{\alpha}(\mathbf{k}, T)$  were fitted to Lorentzian functions at each  $k$ -point and  $T$ ; these fits are seen within the shaded areas in Fig. 2(b) (the background shown within red lines was added to these fits). Phonon lifetimes are given by  $\tau_{l,\alpha}(\mathbf{k}, T) = [\pi\Delta\nu_{\alpha}(\mathbf{k}, T)]^{-1}$ . The average value of  $\tau_{l,\alpha}(\mathbf{k}, T)$  was 2.6 ps across the 100 to 400 K temperature range studied here. The finite-temperature fitted values of  $\nu_{\alpha}(\mathbf{k}, T)$  and  $\tau_{l,\alpha}(\mathbf{k}, T)$  obtained straight from the molecular dynamics evolution will be used to determine the lattice thermal conductivity next.

The power spectra data describe the vibrational frequencies at each temperature and include information on phonon-phonon interactions through broadening of the natural frequencies. This *nonperturbative* process fully incorporates anharmonicity in the phonon frequencies and phonon lifetimes, in contrast to the standard approach [22], in which phonon scattering rates are determined self-consistently in a perturbation series to low-order and added together. Furthermore, the phonon spectrum in Fig. 3(c) reflects the structural transition [16,17,21,29] shown earlier in Fig. 1.

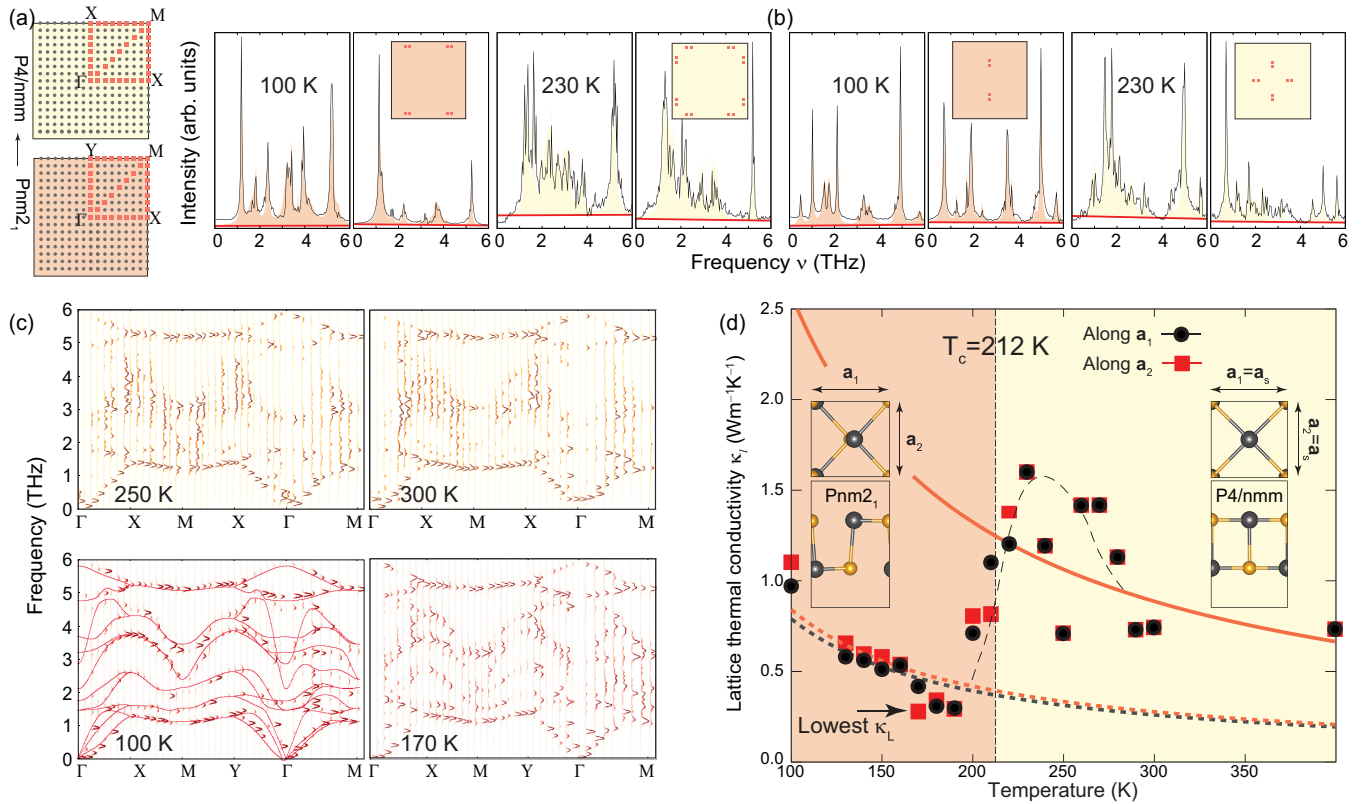


FIG. 3. (a) First Brillouin zone above (square, top) and below (rectangle, bottom)  $T_c$  [16,17]. (b) Power spectra at two consecutive  $k$  points. (c) Phonon spectrum for  $T$  above  $T_c$  (top subplots) and below (lower subplots)  $T_c$  along the red path in (a). Optical phonon modes with frequencies between 2 and 4 THz soften at  $T > T_c$ . Red curves are zero- $T$  phonons as a guide to the eye. (d)  $\kappa_l$  from the phonon spectrum at finite  $T$  along the  $x$  ( $a_1$ , circles) and  $y$  ( $a_2$ , squares) directions. The solid line is the fit to the data above  $T = 190$  K, and the dotted black (red) line is the fit to the data below  $T = 190$  K along the  $a_1 = x$  ( $a_2 = y$ ) direction. The black dashed curve is a guide to the eye, showing the sudden increase in  $\kappa_l$  at and beyond  $T_c$ .

These nonperturbative finite- $T$  vibrational modes profoundly affect  $ZT$ .

Obtaining the lattice thermal conductivity  $\kappa_l$  [Fig. 3(d)] requires the phonon group velocity  $\mathbf{v}_{\text{ph},\alpha}(\mathbf{k}, T)$  calculated by finite difference for the  $\alpha$ th mode at each  $k$  point and  $T$ . This way,  $\kappa_l$  is given by

$$\kappa_{l,ij}(T) = \frac{1}{\Omega(T)} \sum_{\mathbf{k},\alpha} v_{\text{ph},\alpha,i}(\mathbf{k}, T) v_{\text{ph},\alpha,j}(\mathbf{k}, T) \tau_{l,\alpha}(\mathbf{k}, T) \times C_{\text{ph},\alpha}(\mathbf{k}, T), \quad (6)$$

with  $\tau_{l,\alpha}(\mathbf{k}, T)$  being the phonon lifetime and  $C_{\text{ph},\alpha}(\mathbf{k}, T)$  the mode-dependent heat capacity,

$$C_{\text{ph},\alpha}(\mathbf{k}, T) = k_B \left( \frac{h\nu_\alpha(\mathbf{k}, T)}{k_B T} \right)^2 \frac{e^{h\nu_\alpha(\mathbf{k}, T)/k_B T}}{(e^{h\nu_\alpha(\mathbf{k}, T)/k_B T} - 1)^2}. \quad (7)$$

Even though  $C_{\text{ph}}$  is expressed within the harmonic approximation, the velocities and frequencies are obtained from molecular dynamics and are thus “renormalized” in the sense that they include anharmonic contributions by design.

The peak shown in Fig. 3(d) near the transition temperature is reminiscent of the anomalous lattice thermal conductivity experimentally observed in  $\text{SmBaMn}_2\text{O}_6$  single crystals across their structural transition [38]. Here, in the ferroelectric  $Pnm2_1$  phase below  $T_c = 212$  K,  $\kappa_l$  decreases with a  $\alpha T^{-1}$  behavior. There appears to be numerical noise on

$\kappa_l$  at two temperatures near 250 K in our data, likely due to system size and time-sampling limitations. Nevertheless, the lattice thermal conductivity exhibits a sudden increase across and above the transition temperature due to the appearance of soft vibrational modes (that hence increase their phonon group velocities  $\mathbf{v}_{\text{ph},\alpha}$ ). An experimental study of  $\text{Cu}_2\text{Se}$ ,  $\text{Cu}_2\text{S}$ ,  $\text{Ag}_2\text{S}$ , and  $\text{Ag}_2\text{Se}$  has also indicated a substantially reduced lattice thermal conductivity just before the onset of their  $T$ -dependent phase transition [9]. Beyond  $T_c$ , Fig. 3(d) shows the gradual decrease of  $\kappa_l$  with temperature, with the points being the average of the values along the two directions, reflective of the square ( $P4/nmm$ ) symmetry. In agreement with Ref. [10], we find a larger  $\kappa_l$  past  $T_c$  than the usual method, which ignores the structural transition altogether.

Optical phonons have been found to contribute to  $\kappa_l$  substantially [39–41]; in other monochalcogenide systems, the contribution owing to the optical modes can be greater than 20% of the total  $\kappa_l$  [42], and it can be as high as 30% in bulk  $\text{SnSe}$  [43]. Even just on the basis of Eq. (6), the unmitigated increase in the phonon velocities, lifetimes, and softened frequencies dominates the lattice thermal conductivity despite a saturating heat capacity  $C_{\text{ph}}$ . An enhanced  $\kappa_l$  has been attributed to higher-velocity softened phonon modes both in silica [44] and in double-perovskite  $\text{SmBaMn}_2\text{O}_6$  single crystals [38]. The sudden softening of vibrations can be hardly

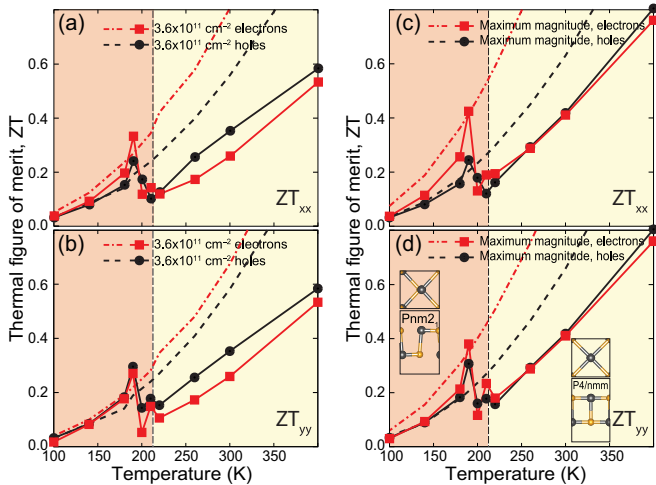


FIG. 4. Thermoelectric figure of merit  $ZT$  for the freestanding SnSe monolayer as a function of  $T$  for electron (hole) doping shown by red rectangles (black circles) within the method presented here. Predictions from the standard method are shown by dash-dotted (dashed) curves for electrons (holes).  $ZT$  for a fixed carrier density of  $3.6 \times 10^{11} \text{ cm}^{-2}$  (a) along the  $x$  ( $a_1$ ) direction and (b) along the  $y$  ( $a_2$ ) direction.  $ZT$  for a varying level of doping which maximizes  $ZT$  (c) along the  $x$  direction and (d) along the  $y$  direction. Note the decreased magnitude of  $ZT$  past  $T_c$ , in contrast to the standard paradigm [15,22] (dashed curves).

accounted for within few-order phonon expansions on a structure at zero temperature [22] (see Refs. [1] and [30]).

$ZT$  is determined along the  $x$  and  $y$  directions in Fig. 4, both for fixed electron or hole densities, and for carrier densities such that  $\mu$  maximizes  $ZT$  at each temperature. Considering the fluctuations seen above  $T_c$  in Fig. 3(d), we used  $\kappa_l$  as determined from the fits above and below  $T_c$  with a resolution of 40 K to calculate  $ZT$  in Fig. 4. We joined these curves using the numerical datapoints for  $\kappa_l$  at 190, 200, and 210 K to highlight the continuity of  $\kappa_l$  across the transition. (The use

of the raw data in Fig. 3(d) will not deny the crucial fact that  $\kappa_l$  increases abruptly across the transition.)  $ZT_{xx} \neq ZT_{yy}$  for all  $T$  within the standard approach to thermoelectricity, due to the use of the rectangular (anisotropic,  $Pnm2_1$ ) ground-state atomistic structure at all temperatures. Using the finite- $T$  data, the thermoelectric figure of merit  $ZT$  is similar to predictions based on zero-temperature data for  $T < 180$  K. Nevertheless,  $ZT$  displays a significant and symmetric drop beyond 190 K, a result in conflict with previous reports on SnSe monolayers in which the structural transition is ignored and which hence overestimate  $ZT$  [14,23,24]. The apparent spike in  $ZT$  near  $T_c$  is similar to the behavior experimentally observed in iodinedoped or alloyed bulk  $\text{Cu}_2\text{Se}$  [45–47].

#### IV. CONCLUSION

In conclusion, we investigated the thermoelectric behavior of a prototypical SnSe monolayer across its two-dimensional ferroelectric-to-paraelectric phase transition, incorporating finite- $T$  MD data to inform both the electronic and lattice thermal behaviors. Both the electronic and vibrational dispersions are signatures of a given material phase, and they necessarily evolve at a phase transition, with necessary modifications to thermoelectric properties, which are usually computed with reference to the zero-temperature phase. Accordingly, we demonstrated that the standard approach to thermoelectricity overestimates  $ZT$  at temperatures above  $T_c$  while introducing a method solely based on finite-temperature molecular dynamics information to predict the dramatic effect of the  $T$ -dependent structural phase transition on  $ZT$ . This method applies to arbitrary thermoelectric materials undergoing solid-to-solid phase transitions in 1, 2, and 3 dimensions.

#### ACKNOWLEDGMENTS

The authors were funded by an Early Career Award from the U.S. DOE (Early Career Award No. DE-SC0016139). Calculations were performed at NERSC, a U.S. DOE User Facility funded under Contract No. DE-AC02-05CH11231.

- [1] A. Zevalkink, D. M. Sniadak, J. L. Blackburn, A. J. Ferguson, M. L. Chabinyk, O. Delaire, J. Wang, K. Kovnir, J. Martin, L. T. Schelhas, T. D. Sparks, S. D. Kang, M. T. Dylla, G. J. Snyder, B. R. Ortiz, and E. S. Toberer, A practical field guide to thermoelectrics: Fundamentals, synthesis, and characterization, *Appl. Phys. Rev.* **5**, 021303 (2018).
- [2] L.-D. Zhao, S.-H. Lo, Y. Zhang, H. Sun, G. Tan, C. Uher, C. Wolverton, V. P. Dravid, and M. G. Kanatzidis, Ultralow thermal conductivity and high thermoelectric figure of merit in SnSe crystals, *Nature (London)* **508**, 373 (2014).
- [3] C. Chang, M. Wu, D. He, Y. Pei, C.-F. Wu, X. Wu, H. Yu, F. Zhu, K. Wang, Y. Chen, L. Huang, J.-F. Li, J. He, and L.-D. Zhao, 3D charge and 2D phonon transports leading to high out-of-plane  $z_t$  in n-type SnSe crystals, *Science* **360**, 778 (2018).
- [4] G. Ding, G. Gao, and K. Yao, High-efficient thermoelectric materials: The case of orthorhombic IV-VI compounds, *Sci. Rep.* **5**, 9567 (2015).
- [5] R. Guo, X. Wang, Y. Kuang, and B. Huang, First-principles study of anisotropic thermoelectric transport properties of IV-VI semiconductor compounds SnSe and SnS, *Phys. Rev. B* **92**, 115202 (2015).
- [6] H. Yu, S. Dai, and Y. Chen, Enhanced power factor via the control of structural phase transition in SnSe, *Sci. Rep.* **6**, 26193 (2016).
- [7] A. Dewandre, O. Hellman, S. Bhattacharya, A. H. Romero, G. K. H. Madsen, and M. J. Verstraete, Two-Step Phase Transition in SnSe and the Origins of Its High Power Factor from First Principles, *Phys. Rev. Lett.* **117**, 276601 (2016).
- [8] P.-C. Wei *et al.*, Thermoelectric figure-of-merit of fully dense single-crystalline SnSe, *ACS Omega* **4**, 5442 (2019).
- [9] H. Chen, Z. Yue, D. Ren, H. Zeng, T. Wei, K. Zhao, R. Yang, P. Qiu, L. Chen, and X. Shi, Thermal conductivity during phase transitions, *Adv. Mater.* **31**, 1806518 (2019).
- [10] M. T. Agne, P. W. Voorhees, and G. J. Snyder, Phase transformation contributions to heat capacity and impact on thermal

- diffusivity, thermal conductivity, and thermoelectric performance, *Adv. Mater.* **31**, 1902980 (2019).
- [11] K. Chang, F. Küster, B. J. Miller, J.-R. Ji, J.-L. Zhang, P. Sessi, S. Barraza-Lopez, and S. S. P. Parkin, Microscopic manipulation of ferroelectric domains in SnSe monolayers at room temperature, *Nano Lett.* **20**, 6590 (2020).
- [12] S. Barraza-Lopez, B. M. Fregoso, J. W. Villanova, S. S. P. Parkin, and K. Chang, Colloquium: Physical behavior of group-IV monochalcogenide monolayers, [arXiv:2009.04341](https://arxiv.org/abs/2009.04341) [Rev. Mod. Phys. (to be published)].
- [13] T. Chattopadhyay, J. Pannetier, and H. Von Schnering, Neutron diffraction study of the structural phase transition in SnS and SnSe, *J. Phys. Chem. Solids* **47**, 879 (1986).
- [14] F. Q. Wang, S. Zhang, J. Yu, and Q. Wang, Thermoelectric properties of single-layered SnSe sheet, *Nanoscale* **7**, 15962 (2015).
- [15] G. K. Madsen and D. J. Singh, BoltzTraP. A code for calculating band-structure dependent quantities, *Comput. Phys. Commun.* **175**, 67 (2006).
- [16] S. Barraza-Lopez, T. P. Kaloni, S. P. Poudel, and P. Kumar, Tuning the ferroelectric-to-paraelectric transition temperature and dipole orientation of group-IV monochalcogenide monolayers, *Phys. Rev. B* **97**, 024110 (2018).
- [17] J. W. Villanova, P. Kumar, and S. Barraza-Lopez, Theory of finite-temperature two-dimensional structural transformations in group-IV monochalcogenide monolayers, *Phys. Rev. B* **101**, 184101 (2020).
- [18] J. M. Soler, E. Artacho, J. D. Gale, A. García, J. Junquera, P. Ordejón, and D. Sánchez-Portal, The SIESTA method for ab initio order-N materials simulation, *J. Phys.: Condens. Matter* **14**, 2745 (2002).
- [19] M. Mehboudi, A. M. Dorio, W. Zhu, A. van der Zande, H. O. H. Churchill, A. A. Pacheco-Sanjuan, E. O. Harriss, P. Kumar, and S. Barraza-Lopez, Two-dimensional disorder in black phosphorus and monochalcogenide monolayers, *Nano Lett.* **16**, 1704 (2016).
- [20] M. Mehboudi, B. M. Fregoso, Y. Yang, W. Zhu, A. van der Zande, J. Ferrer, L. Bellaiche, P. Kumar, and S. Barraza-Lopez, Structural Phase Transition and Material Properties of Few-Layer Monochalcogenides, *Phys. Rev. Lett.* **117**, 246802 (2016).
- [21] S. P. Poudel, J. W. Villanova, and S. Barraza-Lopez, Group-IV monochalcogenide monolayers: Two-dimensional ferroelectrics with weak intralayer bonds and a phosphorenelike monolayer dissociation energy, *Phys. Rev. Mater.* **3**, 124004 (2019).
- [22] W. Li, J. Carrete, N. A. Katcho, and N. Mingo, ShengBTE: A solver of the Boltzmann transport equation for phonons, *Comput. Phys. Commun.* **185**, 1747 (2014).
- [23] Y. Sun, Z. Shuai, and D. Wang, Reducing lattice thermal conductivity of the thermoelectric SnSe monolayer: Role of phonon–electron coupling, *J. Phys. Chem. C* **123**, 12001 (2019).
- [24] G. Ding, Y. Hu, D. Li, and X. Wang, A comparative study of thermoelectric properties between bulk and monolayer SnSe, *Results Phys.* **15**, 102631 (2019).
- [25] Z.-Y. Hu, K.-Y. Li, Y. Lu, Y. Huang, and X.-H. Shao, High thermoelectric performances of monolayer SnSe allotropes, *Nanoscale* **9**, 16093 (2017).
- [26] R. L. González-Romero, A. Antonelli, and J. J. Meléndez, Insights into the thermoelectric properties of SnSe from ab initio calculations, *Phys. Chem. Chem. Phys.* **19**, 12804 (2017).
- [27] C. W. Li, J. Hong, A. F. May, D. Bansal, S. Chi, T. Hong, G. Ehlers, and O. Delaire, Orbitally driven giant phonon anharmonicity in SnSe, *Nat. Phys.* **11**, 1063 (2015).
- [28] C. Chang, G. Tan, J. He, M. G. Kanatzidis, and L.-D. Zhao, The thermoelectric properties of SnSe continue to surprise: Extraordinary electron and phonon transport, *Chem. Mater.* **30**, 7355 (2018).
- [29] K. Chang, J. Liu, H. Lin, N. Wang, K. Zhao, A. Zhang, F. Jin, Y. Zhong, X. Hu, W. Duan, Q. Zhang, L. Fu, Q.-K. Xue, X. Chen, and S.-H. Ji, Discovery of robust in-plane ferroelectricity in atomic-thick SnTe, *Science* **353**, 274 (2016).
- [30] J. Heremans, The anharmonicity blacksmith, *Nat. Phys.* **11**, 990 (2015).
- [31] P. Souvatzis, O. Eriksson, M. I. Katsnelson, and S. P. Rudin, Entropy Driven Stabilization of Energetically Unstable Crystal Structures Explained from First Principles Theory, *Phys. Rev. Lett.* **100**, 095901 (2008).
- [32] O. Hellman, I. A. Abrikosov, and S. I. Simak, Lattice dynamics of anharmonic solids from first principles, *Phys. Rev. B* **84**, 180301(R) (2011).
- [33] A. H. Romero, E. K. U. Gross, M. J. Verstraete, and O. Hellman, Thermal conductivity in PbTe from first principles, *Phys. Rev. B* **91**, 214310 (2015).
- [34] N. Shulumba, O. Hellman, and A. J. Minnich, Lattice Thermal Conductivity of Polyethylene Molecular Crystals from First-Principles Including Nuclear Quantum Effects, *Phys. Rev. Lett.* **119**, 185901 (2017).
- [35] A. J. H. McGaughey, A. Jain, H.-Y. Kim, and B. Fu, Phonon properties and thermal conductivity from first principles, lattice dynamics, and the Boltzmann transport equation, *J. Appl. Phys.* **125**, 011101 (2019).
- [36] R. M. Pick, M. H. Cohen, and R. M. Martin, Microscopic theory of force constants in the adiabatic approximation, *Phys. Rev. B* **1**, 910 (1970).
- [37] E. N. Koukaras, G. Kalosakas, C. Galiotis, and K. Papagelis, Phonon properties of graphene derived from molecular dynamics simulations, *Sci. Rep.* **5**, 12923 (2015).
- [38] L. Chen, Z. Xiang, C. Tinsman, Q. Huang, K. G. Reynolds, H. Zhou, and L. Li, Anomalous thermal conductivity across the structural transition in SmBaMn<sub>2</sub>O<sub>6</sub> single crystals, *Appl. Phys. Lett.* **114**, 251904 (2019).
- [39] T. Shiga, J. Shiomi, J. Ma, O. Delaire, T. Radzynski, A. Lusakowski, K. Esfarjani, and G. Chen, Microscopic mechanism of low thermal conductivity in lead telluride, *Phys. Rev. B* **85**, 155203 (2012).
- [40] T. Beechem, J. C. Duda, P. E. Hopkins, and P. M. Norris, Contribution of optical phonons to thermal boundary conductance, *Appl. Phys. Lett.* **97**, 061907 (2010).
- [41] Z. Tian, K. Esfarjani, J. Shiomi, A. S. Henry, and G. Chen, On the importance of optical phonons to thermal conductivity in nanostructures, *Appl. Phys. Lett.* **99**, 053122 (2011).
- [42] N. Shulumba, O. Hellman, and A. J. Minnich, Intrinsic localized mode and low thermal conductivity of PbSe, *Phys. Rev. B* **95**, 014302 (2017).
- [43] G. Qin, Z. Qin, W.-Z. Fang, L.-C. Zhang, S.-Y. Yue, Q.-B. Yan, M. Hu, and G. Su, Diverse anisotropy of phonon transport

- in two-dimensional group IV–VI compounds: A comparative study, *Nanoscale* **8**, 11306 (2016).
- [44] H. Aramberri, R. Rurali, and J. Íñiguez, Thermal conductivity changes across a structural phase transition: The case of high-pressure silica, *Phys. Rev. B* **96**, 195201 (2017).
- [45] H. Liu, X. Yuan, P. Lu, X. Shi, F. Xu, Y. He, Y. Tang, S. Bai, W. Zhang, L. Chen, Y. Lin, L. Shi, H. Lin, X. Gao, X. Zhang, H. Chi, and C. Uher, Ultrahigh thermoelectric performance by electron and phonon critical scattering in  $\text{Cu}_2\text{Se}_{1-x}\text{I}_x$ , *Adv. Mater.* **25**, 6607 (2013).
- [46] D. Byeon, R. Sobota, K. Delime-Codrin, S. Choi, K. Hirata, M. Adachi, M. Kiyama, T. Matsuura, Y. Yamamoto, M. Matsunami, and T. Takeuchi, Discovery of colossal Seebeck effect in metallic  $\text{Cu}_2\text{Se}$ , *Nat. Commun.* **10**, 72 (2019).
- [47] D. Vasilevskiy, M. K. Keshavarz, J.-M. Simard, R. A. Masut, S. Turenne, and G. J. Snyder, Assessing the thermal conductivity of  $\text{Cu}_{2-x}\text{Se}$  alloys undergoing a phase transition via the simultaneous measurement of thermoelectric parameters by a Harman-based setup, *J. Electron. Mater.* **47**, 3314 (2018).